2020 IEEE/RSJ International Conference on Intelligent Robots and Systems (IROS)
October 25-29, 2020, Las Vegas, NV, USA (Virtual)

Development of a Spherical 2-DOF Wrist Employing Spatial Parallelogram Structure

Hyunhwan Jeong, Sunhyuk Baek, Wheekuk Kim, and Byung-Ju Yi, *Member, IEEE*

***Abstract*—A spherical two-degree-of- freedom wrist adapting the structure of the spatial parallelogram is proposed. A U type extended link out of three UU type limbs of the spatial parallelogram is selected as an output link. As a result, the wrist can be interpreted as being formed by combination of a U type limb and a (2-UU)+U type hybrid limb. Screw theory is employed to analyze its first-order kinematic model. Then a compact wrist prototype suitable for wrist module supporting the robot hand is designed and implemented. Finally, experiments with the prototype confirm that the wrist has a very high potential application for wrist modules in terms of dexterity and maximum load handling capacity.**

I. Introduction

The parallel mechanisms (PMs) have many advantages as compared to the serial manipulators in aspects of rigidity, high precision, low inertia, high payload, etc. Thus, continuous efforts been devoted to develop many useful PMs [1-17]. For last two decades, systematic type synthesis methods to identify various types of the PMs such as constraint-synthesis methods, lie-group displacement method, etc. have been introduced [8-12]. Based on those methods, a large number of multi-Degree-of-freedom (DOF) PMs having a common output platform have been successfully identified, including various types of spherical 2-DOF or 3-DOF PMs.

Specifically, spherical PMs are effective in orienting end-effector such as gripper or robotic hand attached to the distal end of the manipulator. However, most of the 3-DOF wrist structures tend to have small workspace due to the increased constraints, compared to the 2-DOF wrist structures. Indeed, various types of excellent 2-DOF PM wrist structures, which secure the fairly large workspace as well as good kinematic characteristics, have been suggested so far. In [13], most of recent state of art of the wrists including both the spherical 2-DOF prosthetic wrists and the spherical 2-DOF robot wrists have been addressed. Also, a variety of 2-DOF serial wrists categorized as passive, body-powered, or active are addressed and also a variety of active 2-DOF parallel wrists along with active 2-DOF hybrid wrists are summarized.

Recently, a spherical 2-DOF bevel-geared 5mm articulating wrist is suggested for the micro-laparoscopy instrument [14], which is advantageous to the other existing cable-driven instrument wrists in aspects of dexterity and rigidity. Other 2-DOF spherical wrists such as the iCub mk.2 wrist [15] and the quaternion joint wrist [16] are suggested, which are suitable to the tasks requiring the large workspace and the high payload capacity. The iCub mk.2 wrist employing the planetary gear is driven by cables. The quaternion joint mechanism approximates the motion of the spherical 2-DOF rolling joint due to its negligibly small parasitic motion. However, it may not be adequate as an active device. Thus, it was employed as a passive device to drive a mechanism by attaching four cables between the base plate and the moving plate. As a comparative study, six different spherical 2-DOF wrists [16-19] including the gimbal wrist have been investigated on the wrists in aspects of workspace size.

Now, several prominent wrists in aspects of its performance and its structure are discussed. A 2-DOF wrist with both a RR limb and a RRR limb [17] has advantages over the others in aspects of its simple geometry, easiness of its manufacturing, workspace size, and kinematic performance. Here, R denotes the revolute joint. OMNI-wrist III is another excellent structure successfully employed as the laser-beam steering device due to its large workspace [19, 20]. However, it has the relatively complex structure but it produces the translational 2-DOF parasitic motion. Another prominent spherical 2-DOF PM structure is the one suggested by Wu and Carricato [21]. This wrist structure employs the concept of constant-velocity shaft couplings. Geometrically, the wrist has two symmetric 3-RRR type PM structure against the virtual plane in the middle of the wrist on which three coupled constant-velocity shafts lie. Thus, the motion of the lower part of the wrist below the plane is duplicated by the upper part of the wrist above the plane such that the output rotational motion of the wrist is doubled. Consequently, the wrist could secure a large workspace.

Note that most of parallel wrists such as the 5R type wrist [17], the OMNI wrist III [19], etc., could be identified based on the typical synthesis methods suggested in literature, but that the one suggested in [21] may not be easy to come up with the structure from the synthesis methods available. Thus, more research should be done to identify new and practical 2-DOF wrist structures.

This work was supported by the Technology Innovation Program (or Industrial Strategic Technology Development Program) (20001856, Development of robotic work control technology capable of grasping and manipulating various objects in everyday life environment based on multimodal recognition and using tools) funded By the Ministry of Trade, Industry & Energy(MOTIE, Korea).

H. H. Jeong is with the Department of Electro-Mechanical System Engineering, Korea University, Sejong, Korea (email: hyunhwanjeong@korea.ac.kr)

S. H. Baek is a graduate student at the Department of Electro-Mechanical System Engineering, Korea University, Sejong, Korea (email: sunhyuk@korea.ac.kr)

W. K. Kim is with the Department of Electro-Mechanical System Engineering, Korea University, Sejong, Korea (e-mail: wheekuk@korea.ac.kr).

B.-J. Yi is with the Department of Electronic Systems Engineering, Hanyang University, Ansan, Korea (corresponding author, e-mail: bj@hanyang.ac.kr).

Now, note that the planar 1-DOF parallelogram consisting of four revolute joints could be employed as either a 1-DOF translational mechanism or a 1-DOF rotational motion transmission linkage, depending on the selection of its output variable. In fact, the planar 1-DOF parallelogram module is employed as the 1-DOF generalized prismatic joint module to construct the various PMs in the type synthesis [22]. Similarly, the spatial 2-DOF parallelogram structure with three UU type limbs could also be employed as either a 2-DOF translational mechanism or a 2-DOF rotational motion transmission linkage, depending on the selection of its output variables. Here U denotes the universal joint and UU type limb denotes the serial limb composed of two U joints. Note that Gao et al [23] used the spatial parallelogram module as the 2-DOF generalized prismatic joint module to construct various PMs in the type synthesis. In this work, the extended link of one limb among three UU limbs as in Fig. 1(a) is selected as the output link of the spatial parallelogram such that the spatial 2-DOF parallelogram structure be used as the 2-DOF rotational motion transmission linkage. In section II, a brief description of the proposed wrist structure is given. Then its position analysis and its kinematic modeling via screw theory are conducted along with the analysis of its kinematic characteristics. In section III, the prototype is designed and implemented. Then preliminary experiments are conducted to verity its motion capability. Lastly, conclusions are drawn.

II. Spatial Parallelogram Type Wrist

A. Description

Figure 1 shows the proposed 2-DOF wrist. Structure of the wrist is analogous to that of the spatial parallelogram. The spatial parallelogram consists of a ternary plate, a base plate, and three UU limbs connecting them. Note that the output motion of the spatial parallelogram can be characterized as the motion of the ternary plate on the spherical surface but with its fixed orientation in general.

In this work, the structure of the mechanism will be interpreted as combination of two sub-chains; a U type sub-chain and (2-UU)+U type hybrid sub-chain as described in Fig. 1. Here, (2-UU) implies the parallel module composed of two serial UU limbs and (2-UU)+U implies the hybrid sub-chain formed by connecting (2-UU) module and a U joint serially. The extended link of the U type sub-chain is chosen as the output link of the proposed wrist. The output link of the wrist is connected to the base plate via a U joint. And the ternary plate of the (2-UU)+U type hybrid sub-chain is connected to the base through two U joints and there is another U joint at the distal end of (2-UU)+U type hybrid sub-chain. Thus the spherical 2-DOF motion of the output link becomes the output of the 2-DOF wrist, and in (2-UU)+U type hybrid sub-chain, two independent base joints in two U joints connected to the base plate is selected as active inputs.

Now, the geometric parameters of the wrist are described in detail. The U joint at the base plate of each limb is placed at the point, B_o, B_1, and B_2. Similarly, the other U joint of each limb is located at the point, P_o, P_1, and P_2 on the ternary plate. Both the base frame and the output frame of the wrist are defined at B_o, the center of the U joint on the base plate as shown in Fig. 1 and they are denoted as $(\hat{x}_b, \hat{y}_b, \hat{z}_b)$ and $(\hat{x}_t, \hat{y}_t, \hat{z}_t)$, respectively. Without loss of generality, the output displacement vector of the wrist is defined as $\boldsymbol{u} = (\alpha \quad \beta)^T$, which are two rotational angles about the two revolute joints of the U joint located at B_o.

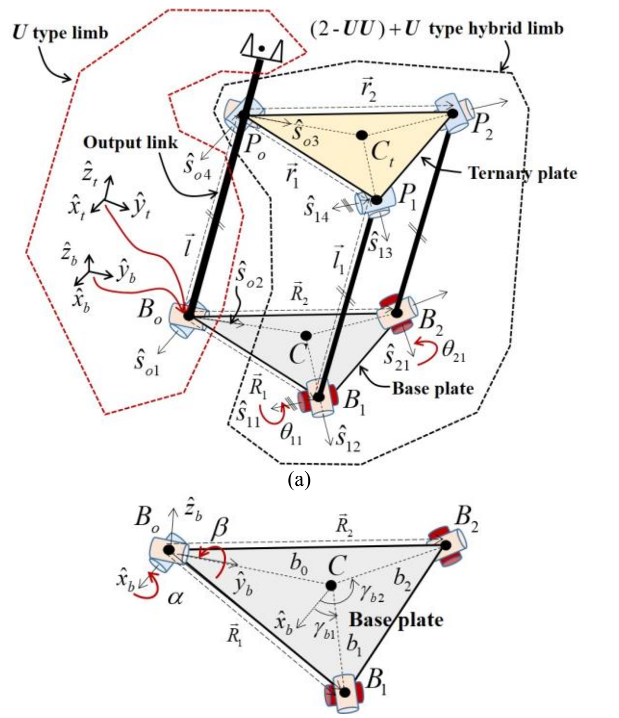

(a)

(b)

Fig. 1. Schematics: (a) the wrist and (b) its base plate parameters (θ_{11} and θ_{21} denote inputs)

The position vector from B_o to P_o is denoted as either $\vec{l}$ or $l\hat{l}$, where $\hat{l}$ denotes the unit vector. Similarly, the other position vectors from B_i to P_i for $i=1,2$ are denoted as either $\vec{l}_i$ or $l_i\hat{l}_i$. As shown in Fig. 1(b), the point C is located away from B_o in the direction of the $\hat{y}_b$ axis and its distance $\overline{B_oC}$ is denoted as b_0. B_i is placed away from the point C with the distance b_i in the direction of an offset angle of γ_{bi} from the $\hat{x}_b$ axis. Similarly, each P_i for $i=1,2$ on the ternary plate is defined in the similar way as B_i on the base plate.

The position vectors $\overrightarrow{B_oB_i}$ and $\overrightarrow{P_oP_i}$ for $i=1,2$ are denoted as $\vec{R}_i$ and $\vec{r}_i$, respectively. θ_{ij} and $\hat{s}_{ij}$ denote the angular displacement and the unit vector along the axis of the *j-th* joint of the *i-th* limb, respectively. θ_{oi} and $\hat{s}_{oi}$ for $i=1,2$ denotes the joint angle and the unit vector along the rotation axis of the U joint connecting the base plate to the output limb, respectively. θ_{oi} and $\hat{s}_{oi}$ for $i=3,4$ denotes the joint angle and the unit vector along the rotation axis of the U joint connecting the ternary plate to the output limb, respectively. The input vector, which consists of the two revolute joints of two U joints connected to the base plate, is denoted as $\boldsymbol{\theta}_a = (\theta_{11} \quad \theta_{21})^T$.

It is assumed that the wrist mechanism satisfies the following geometric conditions: for $i=1,2$, (i) $\gamma_{bi}=\gamma_{ti}$, $|R_i|=|r_i|$ and $\vec{R}_i \parallel \vec{r}_i$, (ii) $l=l_i$, (iii) $\hat{l}_o \parallel \hat{l}_i$, (iv) $\hat{s}_{i1} \parallel \hat{s}_{i4}$ and $\hat{s}_{i2} \parallel \hat{s}_{i3}$, and (v) $\hat{s}_{i1}\times\hat{s}_{i2} \parallel \hat{s}_{i3}\times\hat{s}_{i4}$ and $\hat{s}_{o1}\times\hat{s}_{o2} \parallel \hat{s}_{o3}\times\hat{s}_{o4}$, where || denotes "is parallel to". It is remarked that when the axes of two universal joints of each limb of the wrist are properly installed, two geometric conditions (iv) and (v) are satisfied by the structure of the wrist mechanism.

B. Position Analysis

The unit vector directing from B_o to P_o is expressed as

$$\hat{l} = Rot(\hat{x},\alpha)Rot(\hat{y},\beta)\hat{z}^{(t)} = \begin{pmatrix} s\beta \\ -s\alpha c\beta \\ c\alpha c\beta \end{pmatrix} = \begin{pmatrix} z_x \\ z_y \\ z_z \end{pmatrix} \quad (1)$$

where $\hat{z}^{(t)}=\begin{pmatrix}0 & 0 & 1\end{pmatrix}^T$. And the unit vector directing from B_i to P_i is expressed as

$$\hat{l}_i = Rot(\hat{z}_b,\gamma_{bi})Rot(\hat{x},90^\circ)Rot(\hat{z},\theta_{i1})Rot(\hat{x},90^\circ)$$
$$Rot(\hat{z},\theta_{i2})Rot(\hat{x},90^\circ)\hat{z} = \begin{bmatrix} c\gamma_{bi} & -s\gamma_{bi} & 0 \\ s\gamma_{bi} & c\gamma_{bi} & 0 \\ 0 & 0 & 1 \end{bmatrix}\begin{pmatrix} c\theta_{i1}s\theta_{i2} \\ c\theta_{i2} \\ s\theta_{i1}s\theta_{i2} \end{pmatrix}. \quad (2)$$

Using the geometric conditions that all three vectors of the wrist are parallel (i.e., $\hat{l} = \hat{l}_i, for\ i=1,2$), we have

$$\begin{pmatrix} s\beta \\ -s\alpha c\beta \\ c\alpha c\beta \end{pmatrix} = \begin{bmatrix} c\gamma_{bi} & -s\gamma_{bi} & 0 \\ s\gamma_{bi} & c\gamma_{bi} & 0 \\ 0 & 0 & 1 \end{bmatrix}\begin{pmatrix} c\theta_{i1}s\theta_{i2} \\ c\theta_{i2} \\ s\theta_{i1}s\theta_{i2} \end{pmatrix} \quad (3)$$

Now, in the inverse position analysis, the output angles (α and β) are specified and active joint input angles need to be identified. In that case, (3) could be modified as

$$\begin{pmatrix} c\theta_{i1}s\theta_{i2} \\ c\theta_{i2} \\ s\theta_{i1}s\theta_{i2} \end{pmatrix} = \begin{bmatrix} c\gamma_{bi} & s\gamma_{bi} & 0 \\ -s\gamma_{bi} & c\gamma_{bi} & 0 \\ 0 & 0 & 1 \end{bmatrix}\begin{pmatrix} s\beta \\ -s\alpha c\beta \\ c\alpha c\beta \end{pmatrix} = \begin{pmatrix} z_x^* \\ z_y^* \\ z_z^* \end{pmatrix} \quad (4)$$

From (4), θ_{i2} and θ_{i1} for $i=1,2$ can be obtained as below

$$\theta_{i2} = a\tan 2(\pm\sqrt{(z_x^*)^2+(z_z^*)^2}, z_y^*) \quad (5)$$

$$\theta_{i1} = a\tan 2(\frac{z_z^*}{s\theta_{i2}},\frac{z_x^*}{s\theta_{i2}}), \quad (\because \theta_{i2} \neq \pm n\pi). \quad (6)$$

In the forward position analysis, two input joint angles are specified and the output angles (α and β) need to be obtained. The first row in (3) for $i=1,2$ yields

$$c\gamma_{b1}c\theta_{11}s\theta_{12} - s\gamma_{b1}c\theta_{12} = c\gamma_{b2}c\theta_{21}s\theta_{22} - s\gamma_{b2}c\theta_{22} \quad (7)$$

and the second row in (3) for $i=1,2$ yields

$$s\gamma_{b1}c\theta_{11}s\theta_{12} + c\gamma_{b1}c\theta_{12} = s\gamma_{b2}c\theta_{21}s\theta_{22} + c\gamma_{b2}c\theta_{22} \quad (8)$$

From (7) and (8), θ_{12} and θ_{22} could be obtained numerically. By inserting those values into (3), the desired output variables (α and β) can be found as below

$$\beta = a\tan 2(z_x,\pm\sqrt{z_y^2+z_z^2}),\ \alpha = a\tan 2(\frac{-z_y}{c\beta},\frac{z_z}{c\beta}) \quad (9)$$

Note that when $\gamma_{b1}=90^\circ$ (i.e., $\hat{s}_{11} \parallel \hat{s}_{o1}$), the closed form of the forward position solution of the wrist exists.

C. Kinematic Modeling

The output velocity of the wrist, $\$_u = \begin{pmatrix}\vec{\omega} & \vec{v}\end{pmatrix}$, can be expressed in two different forms. The output velocity of the wrist with respect to the U type sub-chain of Fig. 1 is expressed as

$$\$_u = \dot{\alpha}\hat{\$}_\alpha + \dot{\beta}\hat{\$}_\beta, \quad (10)$$

where

$$\hat{\$}_\alpha = \begin{pmatrix}\hat{x}_b & \mathbf{0}\end{pmatrix},\ \hat{\$}_\beta = \begin{pmatrix}\hat{y}_t & \mathbf{0}\end{pmatrix} \quad (11)$$

The output velocity of the wrist with respect to the (2-UU)+U type hybrid sub-chain is expressed as

$$\$_u = \sum_{j=1}^{4}\dot{\theta}_{ij}\hat{\$}_{ij} + \sum_{k=3}^{4}\dot{\theta}_{ok}\hat{\$}_{ok}, for\ i=1,2 \quad (12)$$

The first summation term in the RHS of (12) denotes the summation of all the joint screws of the *i-th* UU limb connected to the ternary plate and the second summation term denotes the summation of joint screws of the U joint at the point P_o .

The actuation wrench corresponding to the active joint of the *i-th* limb can be obtained as a reciprocal screw to all joints except the corresponding active joint of the limb. In particular, two UU limbs of (2-UU)+U type hybrid sub-chain are constrained such that the second joint rate and the third joint rate have the same magnitude but with opposite sign (i.e., $\dot{\theta}_{i2}=-\dot{\theta}_{i3}$) and their axes are parallel (i.e., $\hat{s}_{i2} \parallel \hat{s}_{i3}$). Thus, the second and third joint screws of the limb can be combined and represented as an equivalent joint screw as below

$$\dot{\theta}_{i2}\hat{\$}_{i2} + \dot{\theta}_{i3}\hat{\$}_{i3} = \dot{\theta}_{i2}\hat{\$}_{i2} - \dot{\theta}_{i2}\hat{\$}_{i3} = \dot{\theta}_{i2}\$_{i23} \quad (13)$$

where $\$_{i23} = \hat{\$}_{i2} - \hat{\$}_{i3} = \begin{pmatrix}0 & \hat{s}_{i2}\times\vec{l}\end{pmatrix}$. Thus, with the substitution of this condition, (12) can be modified as below

$$\$_u = \dot{\theta}_{i1}\hat{\$}_{i1} + \dot{\theta}_{i2}\$_{i23} + \dot{\theta}_{i4}\hat{\$}_{i4} + \sum_{k=3}^{4}\dot{\theta}_{ok}\hat{\$}_{ok}, for\ i=1,2 \quad (14)$$

Now, the actuation wrench corresponding to each of two active joints can be identified as Fig. 3 by finding the reciprocal screw to four remaining joint screws excluding the active joint screw in RHS of (14) as below

$$\hat{\$}_{i1}^{AW} = \begin{pmatrix}\hat{s}_{i1}^{AW} & \vec{r}_{i1}^{AW}\times\hat{s}_{i1}^{AW}\end{pmatrix}\ ,\ for\ i=1,2 \quad (15)$$

where $\vec{r}_{i1}^{AW}=\vec{l}$ and $\hat{s}_{i1}^{AW} \parallel (\hat{s}_{i2}\times\vec{l})\times(\vec{r}_i\times\hat{s}_{i4})$. ($\vec{r}_{i1}^{AW}=\vec{l}$) implies that the axis of $\hat{\$}_{i1}^{AW}$ intersects the point P_o . ($\hat{s}_{i1}^{AW} \parallel (\hat{s}_{i2}\times\vec{l})\times(\vec{r}_i\times\hat{s}_{i4})$) implies that the axis of the $\hat{s}_{i1}^{AW}$ is parallel to the intersection between two planes: one plane ($\prod_{\hat{s}_{i2}-\vec{l}}$) where both $\hat{s}_{i2}$ and $\vec{l}$ lie (i.e., $\hat{s}_{i2}\times\vec{l}\cdot\hat{s}_{i1}^{AW}=0$) and the other plane ($\prod_{\hat{s}_{i4}-\vec{r}_i}$), where both $\hat{s}_{i4}$ and $\vec{r}_i$ lie (i.e., $\vec{r}_i\times\hat{s}_{i4}\cdot\hat{s}_{i1}^{AW}=0$).

The orthogonal product operations between the actuation wrench $\hat{\$}_{i1}^{AW}$ in (15) and both sides of motion screws in (14) yield the following kinematic equations

$$\hat{\$}_{i1}^{AW} \circ \$_u = \hat{\$}_{i1}^{AW} \circ \dot{\theta}_{i1}\hat{\$}_{i1}. \tag{16}$$

By substituting both (10) and (15) into (16), velocity equation of the wrist with respect to the x-y Euler's rate vector $\dot{\boldsymbol{\mu}}_{\alpha\beta} = \begin{pmatrix}\dot{\alpha} & \dot{\beta}\end{pmatrix}^T$ can be found as follows:

$$A_{\alpha\beta}\dot{\boldsymbol{\mu}}_{\alpha\beta} = B_{\alpha\beta}\dot{\boldsymbol{\theta}}_a \tag{17}$$

where

$$\mathrm{A}_{\alpha\beta} = \begin{bmatrix} \hat{l}\times\hat{s}_{11}^{AW}\cdot\hat{x}_b & \hat{l}\times\hat{s}_{11}^{AW}\cdot\hat{y}_t \\ \hat{l}\times\hat{s}_{21}^{AW}\cdot\hat{x}_b & \hat{l}\times\hat{s}_{21}^{AW}\cdot\hat{y}_t \end{bmatrix} \tag{18}$$

$$B_{\alpha\beta} = \begin{bmatrix} -\hat{l}\cdot\hat{s}_{11}\times\hat{s}_{11}^{AW} & 0 \\ 0 & -\hat{l}\cdot\hat{s}_{21}\times\hat{s}_{21}^{AW} \end{bmatrix} \tag{19}$$

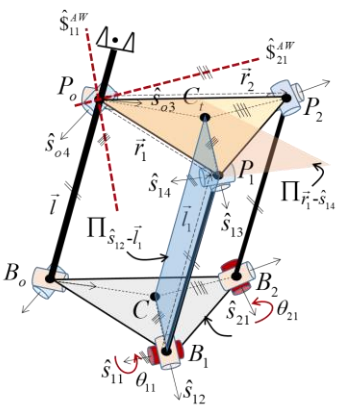

Fig. 3. Actuation wrench

When $A_{\alpha\beta}$ is invertible, the forward velocity equation can be expressed as

$$\dot{\boldsymbol{\mu}}_{\alpha\beta} = J_{\alpha\beta}\dot{\boldsymbol{\theta}}_a, \tag{20}$$

where

$$J_{\alpha\beta} = A_{\alpha\beta}^{-1}B_{\alpha\beta}. \tag{21}$$

When $B_{\alpha\beta}$ is invertible, the inverse velocity equation can be expressed as

$$\dot{\boldsymbol{\theta}}_a = J_{\alpha\beta}^{-1}\dot{\boldsymbol{\mu}}_{\alpha\beta}, \tag{22}$$

where

$$J_{\alpha\beta}^{-1} = B_{\alpha\beta}^{-1}A_{\alpha\beta}. \tag{23}$$

Now, denote the output torque vector about the joint axes of two output Euler angles (α and β) as $\boldsymbol{f}_{\alpha\beta} = \begin{pmatrix}\tau_\alpha & \tau_\beta\end{pmatrix}^T$. By applying the principle of virtual work to (22), the force equation between input torque vector $\boldsymbol{f}_{\alpha\beta}$ and output torque vector $\boldsymbol{\tau}_a$ can be obtained as

$$\boldsymbol{f}_{\alpha\beta} = J_{\alpha\beta}^{-T}\boldsymbol{\tau}_a. \tag{24}$$

D. Kinematic Characteristics

Kinematic characteristic of the wrist can be represented via kinematic isotropy (KI) index, which is defined as below

$$\sigma_{KI} = \frac{\sigma_{\min}(J_{\alpha\beta})}{\sigma_{\max}(J_{\alpha\beta})} \tag{25}$$

where $\sigma_{\max}$ and $\sigma_{\min}$ denotes the maximum singular value and the minimum singular value of $J_{\alpha\beta}$ in (25), respectively. Also, the maximum load capacity of the wrist, which is defined as the minimum singular value of the inverse-transpose of the Jacobian, is denoted as $\sigma_{\min}(J_{\alpha\beta}^{-T})$. Maximum load handling capacity (MLHC) index is defined as the maximum payload which could exert to all directions at the current configuration for the given unit input torque. The larger the two indices, the better the performance.

Due to simple geometry of the proposed spatial parallelogram type wrist, design parameters to consider is not many. As shown in (17)~(19), all link lengths and the position vectors related to the locations of the joints, $\vec{r}_i$, *for* $i = 1,2$, have also no effects on the kinematic characteristics. However, they may cause mechanical interferences. That is, kinematic characteristics of the wrist are the same, irrespective of the values of three parameters: l, b_o, and $b_1 = b_2 \neq 0$. Thus, design parameters of the proposed wrist are the offset angles of both the base plate and the ternary plate. Through several simulations, optimal offset angles could be easily identified as follows: (i) the offset angles between two active joints are perpendicular (i.e., $\gamma_{b2} - \gamma_{b1} = \pm 90^\circ$) and (ii) one offset angle is aligned to the first passive axis of the U joint of the output link (i.e., either $\gamma_{b1} = \pm 90^\circ$ or $\gamma_{b2} = \pm 90^\circ$).

In the following simulations, all link lengths are set equal (i.e., $l = l_i$, *for* $i = 0,1,2$). And the offset angles of the base plate are set as $\gamma_{b2} - \gamma_{b1} = \pm 90^\circ$. Now, the kinematic characteristics of the wrist are analyzed. Figure 4(a) and 4(b) show the contour plots of the KI index and the MLHC index of the proposed wrist, respectively. From the figures, it can be seen that the proposed wrist has fairly good kinematic isotropy property throughout the workspace and also has the fairly good and uniform maximum load handling capacity around the center of its workspace.

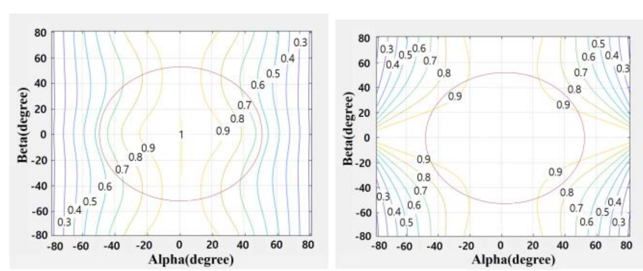

(a) (b)

Fig. 4. (a) KI index and (b) MLHC index w.r.t. $\dot{\boldsymbol{\mu}}_{\alpha\beta}$

III. Prototype Implementation

A. Prototype Design

Figure 5 shows the final design of the prototype. Main objectives of the design are (i) to make the wrist size compact such that it could be employed as the 2-DOF wrist module of the manipulator, (ii) to secure the large workspace as possible,

(iii) to secure the structural rigidity of the wrist, and (iv) to secure the hollow space in the middle of the wrist such that wires could be placed.

To secure the large workspace by minimizing mechanical interferences among the UU limbs and both plates, the length of the link (l) is selected as 34*mm*. The universal joint of each of two UU-limbs on the base plate is located on the same circle of the radius $b_1 = b_2 = r_b$ with the difference of 90° between two offset angles ($\Delta\gamma_{b21} = \gamma_{b2} - \gamma_{b1}$). However, the location of the universal joint of the output link on the base plate is located away from the center of the same circle with the offset distance b_0 as shown in Fig. 1(b). Thus, selected offset angles are $\gamma_{b1} = 45^\circ$ and $\gamma_{b2} = 135^\circ$. In addition, to avoid the mechanical interference between the wrist module and the hand which would be attached to the end of the wrist prototype, a mounting plate is attached to the upper end of the wrist module as shown in Fig. 5. The length of the mounting plate (L_2) is selected as 73.5*mm* which is defined as the distance from the wrist point to the outer surface of the mounting plate where the robot hand would be attached. Design parameters of the prototype is summarized in Table I. The workspace of the prototype is $-48^\circ \le \alpha \le 53^\circ$ and $-53^\circ \le \beta \le 53^\circ$. The structural analysis of the prototype was performed through *Ansys* software under the desired payload and its rigidity was verified.

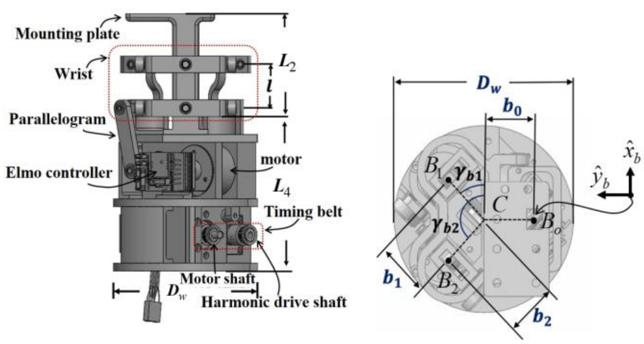

(a) (b)

Fig. 5. Final design of the wrist prototype: (a) side view and (b) top view

TABLE I. DESIGN PARAMETERS OF THE PROTOTYPE WRIST

Design parameters	Specifications
Link length of the UU limb	$l = 34mm$
Radius of base circle	$r_o = b_1 = b_2 = 34.14mm$
Offset distance on the base	$b_o = 29.04mm$
Offset angles on the base	$\gamma_{b1} = 45^\circ$, $\gamma_{b2} = 135^\circ$
Length of mounting plate	$L_2 = 73.5mm$
Height of the base body	$L_4 = 126.5mm$
Outer diameter of the wrist	$D_w = 120mm$

B. Experiments

Figure 7 shows the hardware interface diagram. Each of two actuators consists of a Maxon motor equipped with both an incremental encoder and a harmonic drive with the gear ratio of $100:1$. It is position-controlled by Elmo controller where the control output signal is sent to the motor based on the encoder signal received as shown in Fig. 7. A PC is used as a main controller and the communication between the PC and the Elmo motion controller is made through the EtherCAT with the real-time control software package TwinCAT. The sampling rate of the wrist in control is around 1KHz.

Figure 8 shows the developed prototype hardware system. It is implemented based on the design parameters in Table I. All motor controllers and harmonic drives are installed right below the base plate of the wrist. Each of two motor outputs is transmitted to the harmonic drive through the timing belt and again the output of the harmonic drive is transmitted to the active joint of the wrist through the four-bar parallel transmission linkage. And Fig. 9(a)~9(e) show its various output poses (α, β) roughly illustrating its workspace size.

Several experiments with the implemented prototype system are conducted to verify its motion capability under the payload. Fig. 10(a) and 10(b) show two different experimental results of the prototype each of which is commended to follow the specified trigonometric trajectory under the payload of $30N$, respectively, as shown below

$$\alpha_d(t) = A\sin(\omega t), \quad \beta_d(t) = 0 \tag{26}$$

$$\alpha_d(t) = 0, \quad \beta_d(t) = A\sin(\omega t) \tag{27}$$

where $A = 35^\circ$ and $\omega = 2\pi/10$ (rad). In Fig. 10(a) and 10(b), θ_{11} and θ_{21} denote the active joint angles of the wrist corresponding to the output angles α and β. And Fig. 11(a) and 11(b) show the angular displacement errors along the same trajectories of Fig. 10(a) and 10(b), respectively. It can be observed from the plots that depending on the configuration of the prototype the magnitudes of the errors seem to be varying a little. However, as a whole, the prototype turns out to follow the specified trajectory successfully within the angular position errors of less than $\pm 0.002rad$.

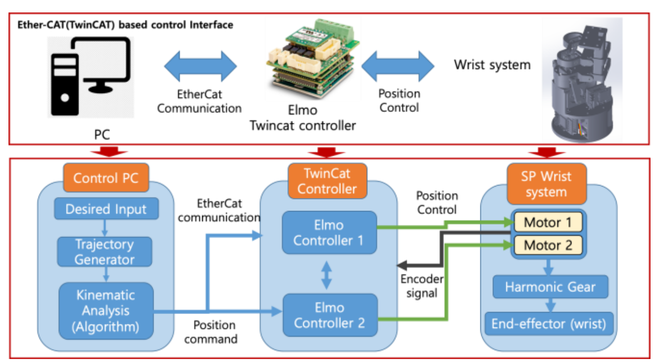

Fig. 7. Hardware interface diagram

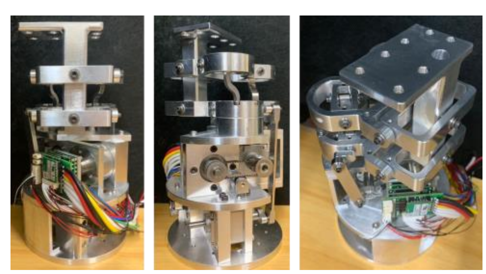

Fig. 8. Prototype hardware

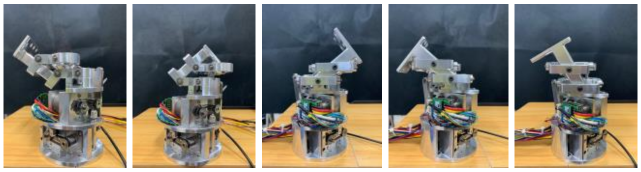

(a) (b) (c) (d) (e)

Fig. 9. Wrist poses: (α,β) : (a) $(\alpha_{\max}=53^{\circ},0^{\circ})$, (b) $(\alpha_{\min}=-48^{\circ},0^{\circ})$, (c) $(0^{\circ},\beta_{\max}=53^{\circ})$, (d) $(0^{\circ},\beta_{\min}=-53^{\circ})$, (e) $(\alpha=40^{\circ},\beta=-50^{\circ})$

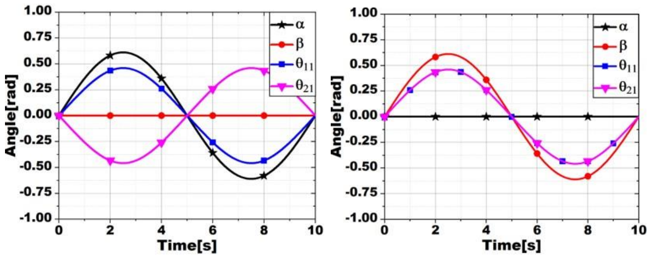

(a) (b)

Fig. 10. Motion trajectories with external load $30N$: (a) $(\alpha(t),\ \beta(t)=0^{\circ})$ and (b) $(\alpha(t)=0^{\circ},\ \beta(t))$

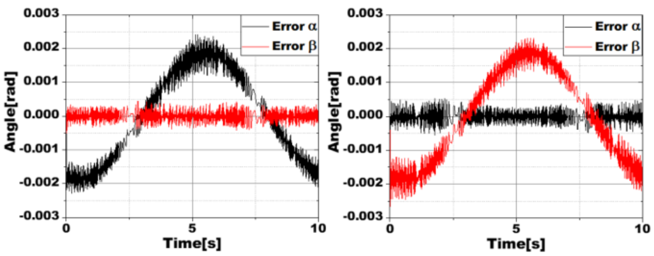

(a) (b)

Fig. 11. Angular displacement errors (a) $(\alpha(t),\ \beta(t)=0^{\circ})$ and (b) $(\alpha(t)=0^{\circ},\ \beta(t))$

IV. Conclusion

A spherical 2-DOF wrist employing the spatial parallelogram structure is suggested and implemented. The wrist structure is geometrically simple such that its kinematic analysis is relatively simple. Screw theory was beneficially employed in the first-order kinematic modeling of the proposed wrist. Through the analysis of the kinematic characteristics of the wrist, it is shown that the wrist has fairly good performance in aspects of both kinematic isotropy and maximum load handling capability. Also, through the development of the simulator it is confirmed that the wrist has fairly large workspace for the wrist application. Lastly, a compact prototype is implemented and it is shown through several motion experiments that the suggested wrist has its very higher potential as a spherical 2-DOF wrist module of the manipulator as compared to existing wrist devices. Future work involves integration of the wrist into robotic hand and screw theory based geometric analysis [24] of the wrist for optimal design.

References

[1] L. Birglen, C. Gosselin, N. Pouliot, B. Monsarrat, and T. Laliberté, “SHaDe, A New 3-DOF Haptic Device,” *IEEE Trans. on Robotics and Automation*, vol. 18, no. 2, 2002, pp. 643-647.

[2] C. Gosselin, E. St-Pierre, and M. Gagn´e, “On the Development of the Agile Eye: Mechanical Design, Control Issues and Experimentation,” *IEEE Robotics and Automation Magazine*, vol. 3, no. 4, 1996, pp. 29-37.

[3] P. Vischer and R. Clavel, “Argos: A Novel 3-DoF Parallel Wrist Mechanism,” *Int. Journal of Robotics Research*, vol. 19, no. 1, 2000, pp. 5-11.

[4] M. Carricato and V. Parenti-Castelli, “A Novel Fully Decoupled 2-DOF Parallel Wrist,” *Int. Journal of Robotics Research*, vol. 23, no. 6, 2004, pp. 661-667.

[5] M. Grebenstein, et. al., “The DLR Hand Arm System,” in Proc. of *IEEE Int. Conf. on Robotics and Automation*, 2011, pp. 3175-3182.

[6] F. L. Hammond III, R. D. Howe, and R. J. Wood, “Dexterous High-Precision Robotic Wrist for Micromanipulation,” in Proc. of *Int. Conf. on Advanced Robotics*, 2013, pp. 1-8.

[7] F. Gao, W. Li, X. Zhao, Z. Jin, and H. Zhao, “New Kinematic Structures for 2-, 3-, 4-, and 5-DOF Parallel Manipulator Designs,” *Mechanism and Machine Theory*, vol. 37, 2002, pp. 1395-1411.

[8] Z. Huang and Q. C. Li, “Type Synthesis of Symmetrical Lower-Mobility Parallel Mechanisms Using the Constraint Synthesis Methods,” *Int. Journal of Robotics Research*, vol. 22, no. 1, 2003, pp. 59-79.

[9] Q. Li, Z. Huang, and J. M. Herve, “Type Synthesis of 3R2T 5-DOF Parallel Mechanisms Using the Lie Group of Displacements,” *IEEE Trans. on robotics and automation*, vol. 20, no. 2, 2004, pp. 173-180.

[10] M. Karouia and J. M. Hervé, “Asymmetrical 3-DOF Spherical Parallel Mechanisms,” *European Journal of Mechanics A*, vol. 24, 2005, pp. 47-57.

[11] X. Kong, and C. M. Gosselin, *Type Synthesis of Parallel Mechanisms*, vol. 33. Springer, 2007.

[12] Z. Huang, Q. C. Li, and H. F. Ding, *Theory of Parallel Mechanisms*, Springer, New York 2012.

[13] N. M. Bajaj, A. J. Spiers, and A. M. Dollar, “State of the Art in Artificial Wrists: A Review of Prosthetic and Robotic Wrist Design,” *IEEE Transactions on Robotics,* vol. 35, no. 1, 2019, pp. 261-277.

[14] J. W. Kim , H.-T. Han , S. C. Kang, and C. W. Kim, “Development of Novel Bevel-Geared 5 mm Articulating Wrist for Micro-Instrument,” *IEEE Robotics and Automation Letters*, vol. 4, no. 4, 2019. Pp. 3711-3718.

[15] D. Shah, Y. Wu, A. Scalzo, G. Metta and A. Parmiggiani, “A Comparison of Robot Wrist Implementations for the iCub Humanoid,” *Robotics*, 2019, vol. 8, no. 11, 2019, doi:10.3390/robotics8010011.

[16] Y. J. Kim, J. I. Kim, Jang, W. Jang, “Quaternion Joint: Dexterous 3-DOF Joint representing quaternion motion for high-speed safe interaction,” In Proceedings of the 2018 IEEE/RSJ International Conference on Intelligent Robots and Systems (IROS), 2018, pp. 935–942.

[17] C. M., Gosselin and F. Caron, “Two Degree-of-Freedom Spherical Orienting Device, US Patent 5,966,991, 1999.

[18] Ueda, K.; Yamada, H.; Ishida, H.; Hirose, S. Design of Large Motion Range and Heavy Duty 2-DOF Spherical Parallel Wrist Mechanism. J. Rob. Mechatron. 2013, 25, 294–305.

[19] M. E. Rosheim and G. F. Sauter, "New High-Angulation Omni-Directional Sensor Mount," in Proc. of *SPIE Conf.,* Seattle, 2002.

[20] J. Sofka, V. Skormin, V. Nikulin, S. Binghamton, and D. J. Nicholson, "Omni-Wrist III–A New Generation of Pointing Devices Part I: Laser Beam Steering Devices–Mathematical Modeling," *IEEE Trans. on Aerospace and Electronic Systems*, vol. 42, no. 2, 2006, pp. 718-725.

[21] Y. Wu and M. Carricato, “Design of a Novel 3-DOF Serial-Parallel Robotic Wrist: A Symmetric Space Approach,” In Proc. *of Int. Symposium on Robotics Research*, 2015, Italy.

[22] X.-J. Liu and J. Wang, “Some New Parallel Mechanisms Containing the Planar Four-Bar Parallelogram,” *Int. Journal of Robotics Research*, vol. 22, no. 9, 2003, pp. 717-732.

[23] F. Gao, W. Li, X. Zhao, Z. Jin, and H. Zhao, “New Kinematic Structures for 2-, 3-, 4-, and 5-DOF Parallel Manipulator Designs,” *Mechanism and Machine Theory*, vol. 37, 2002, pp. 1395-1411.

[24] H. Iqbal, M.U.A. Khan, B.-J. Yi, “Analysis of Duality-based Interconnected Kinematics of Planar Serial and Parallel Manipulators Using Screw Theory,” *Intelligent. Service Robotics*, vol. 13, no. 1, 2020, pp. 47-62.